Research Article | Vol. 12, No. 7 / 1 Jul 2022 / Optical Materials Express 2772

Optical Materials EXPRESS

Method to measure the refractive index for photoluminescence modelling

ELISE BAILLY,[1] KEVIN CHEVRIER,[2] CAMILO PEREZ DE LA VEGA,[2] JEAN-PAUL HUGONIN,[1] YANNICK DE WILDE,[2] VALENTINA KRACHMALNICOFF,[2] BENJAMIN VEST,[1] AND JEAN-JACQUES GREFFET[1,*]

[1] *Universite Paris-Saclay, Institut d'Optique Graduate School, CNRS, Laboratoire Charles Fabry, 91127, Palaiseau, France*
[2] *Institut Langevin, ESPCI Paris, Université PSL, CNRS, 75005 Paris, France*
[*] *jean-jacques.greffet@institutoptique.fr*

Abstract: Light emission by fluorophores can be computed from the knowledge of the absorption spectrum. However, at long wavelengths, the calculated emission may diverge if the decay of the imaginary part of the permittivity is not modelled with precision. We report a technique to obtain the permittivity of fluorophores such as dye molecules from fluorescence measurements. We find that the Brendel-Bormann model enables to fit the emission spectra accurately.

© 2022 Optica Publishing Group under the terms of the Optica Open Access Publishing Agreement

1. Introduction

Fluorophores such as rare earth ions, dye molecules or quantum dots are widely used for lighting applications. They can be coupled to resonant metasurfaces in order to control the emission properties. Metasurfaces can be used to improve light extraction [1–21], to control the emission spectrum [22–27] or the directivity [28–34]. Novel light-matter interaction regimes have been explored in these platforms including strong coupling [35–42] and Bose-Einstein condensation [43,44]. A summary can be found in recent reviews [13,45]. As discussed in the reviews, the interplay between the emitters and the metasurface is accounted for by modelling the emitters as individual electric dipoles randomly oriented inside the structure whose contributions can be added incoherently. The dipole emission spectrum is taken to be the emission spectrum of the emitters which accounts for the Stokes shift compared to the absorption spectrum. Such an approach yields the power emitted by a metasurface up to a proportionality factor related to the excitation. It is therefore not quantitative and cannot be used to model the efficiency of the source. A quantitative model should include a description of the temperature dependent population of the electronic states.

In related systems, such as light emitting diodes (LEDs), a statistical approach is routinely used to establish a model of light emission. Indeed, the emitted power can be given quantitatively by a generalized Kirchhoff law [46,47]. This relation states that the emitted flux is given by the product of the absorptivity of the device and the blackbody radiance. The latter depends on the temperature T and on a so-called photon chemical potential denoted by μ which is the difference of the quasi-Fermi levels in the conduction band and the valence band. For LEDs, μ is equal to eV where e is the electron charge and V is the voltage applied to the diode by the driving electrical source. Therefore, maximizing the light emission by a given system can be achieved by maximizing its absorptivity in the active region. Besides, this model yields an upper bound of the emitted power. This figure of merit is useful when considering metasurface design and efficiency optimization. A record-efficiency light emitting diode [48] has been designed following this approach. In principle, the same approach could also be used for fluorophores coupled to resonant metasurfaces. However, this method has not been reported so far. As will be

#461515 https://doi.org/10.1364/OME.461515
Journal © 2022 Received 18 Apr 2022; revised 16 May 2022; accepted 31 May 2022; published 24 Jun 2022

Optical Materials EXPRESS

shown below, a key difficulty to be addressed is the introduction of a suitable permittivity model for the fluorophores. The purpose of this article is to solve this outstanding issue.

For many applications such as reflectivity measurements in the strong coupling regime [35,36,49], the permittivity of the fluorophores is modelled using a Lorentzian model. These fits are often in great agreement with experimental data from reflectivity measurements. However this Lorentzian model fails to retrieve the experimental photoluminescence using Kirchhoff law, as it can be seen in Fig. 1. More sophisticated models of the permittivity include a sum of Lorentzian lines, or a sum of poles [50–53]. These models suffer from the same drawback and do not enable to retrieve the experimental photoluminescent emission. Hence, there is a need to identify an alternative model of the permittivity to enable the use of Kirchhoff law to compute photoluminescence.

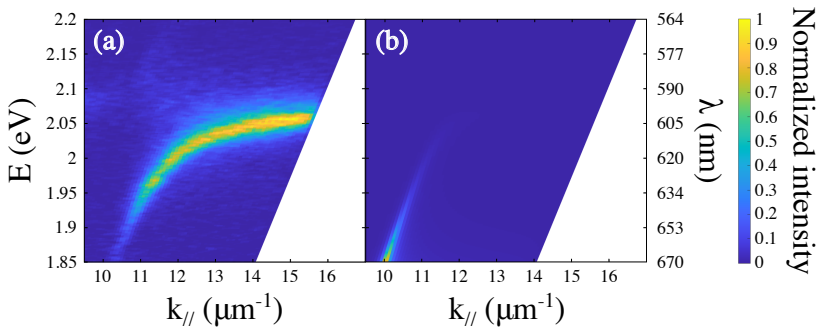

Fig. 1. Maps of photoluminescence as a function of the energy and the parallel wave-vector, normalized by their maximum values: (a) Experimental photoluminescent emission of TDBC (b) Simulated emission using Kirchoff law and a Lorentzian model. This model is defined as follows: $\epsilon_{\mathrm{L}}(\omega) = n_0^2 + \dfrac{f_{\mathrm{L}}}{E_{\mathrm{a}}^2 - \omega^2 - i\omega\gamma_{\mathrm{L}}}$ with $f_{\mathrm{L}} = 0.55\ \mathrm{eV}^2$, $n_0 = 1.65$, $E_{\mathrm{a}} = 2.09$ eV and $\gamma_{\mathrm{L}} = 0.027$ eV. These parameters were fitted from the experimental reflectivity map of Fig. 3(b). All data are normalized.

In this article, we show that the Brendel-Bormann model [54–56] can be used successfully. It corresponds to an infinite sum of Lorentz oscillators whose amplitudes are given by a Gaussian function centered on the transition frequency. If necessary, the model can be improved by adding other infinite sums of oscillators, centered at different frequencies.

To quantitatively assess the fundamental connection between the absorption and emission, we use the relation $\sigma_{em}(\omega) = \sigma_{abs}(\omega)\exp[\hbar(\mu - \omega)/k_B T]$ where σ_{em} is the emission cross section, σ_{abs} is the absorption cross section, and μ is the photon chemical potential which accounts for the pumping. The presence of the exponential factor $\exp(-\hbar\omega/k_B T)$ is responsible for the red shift of the emission spectrum known as Stokes shift. This relation has been derived by several authors for systems in equilibrium ($\mu = 0$) and later extended to account for pumping (see e.g. [57,58] and references therein for a discussion of earlier contributions by Kennard, Stepanov, Neporent and McCumber). A related relation is the fluctuation-dissipation theorem which connects the power spectral density of the current fluctuations (i.e. the source of emission) to the imaginary part of the permittivity of the material. A generalized form of this theorem valid for a non-zero chemical potential has been reported in Ref. [59]. Knowing the absorption cross section, it is possible in principle to use this relation to compute the emission cross section and retrieve the experimental Stokes shift. This relation can be used as a simple test of a permittivity model. To proceed, we write the absorptivity coefficient using either the refractive index n, $\kappa_{abs} = 2\mathrm{Im}(k) = 2\mathrm{Im}(n)\omega/c$ or using the absorption cross section: $\kappa_{abs} = N\sigma_{abs}$ where N is the number of fluorophores per

Optical Materials EXPRESS

unit volume. Therefore, we obtain that $\sigma_{abs} \propto \mathrm{Im}(n)$. The spectra of Fig. 2 were obtained in this way, for a Brendel-Bormann model (Fig. 2(a)) or for a Lorentzian model (Fig. 2(b)).

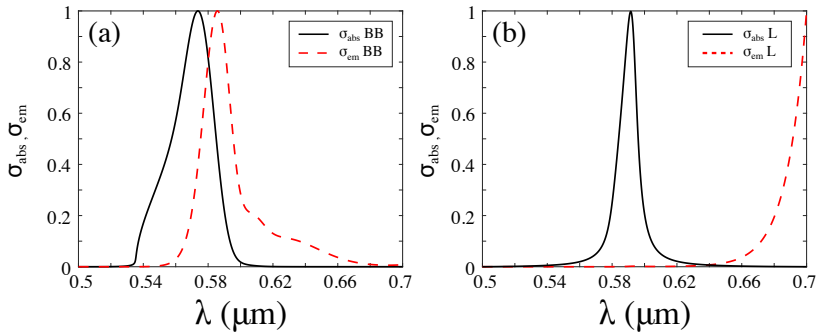

Fig. 2. Emission and absorption cross sections for TDBC, computed with (a) the Brendel-Bormann or (b) the Lorentzian model of permittivity. The Brendel-Bormann model is defined in Eq. (5) and the associated parameters are gathered in Table 1. The Lorentzian model is defined in Fig. 1. We observe that the Brendel-Bormann model reproduces properly the Stokes shift between absorption and emission whereas the Lorentzian model fails to properly reproduce the spectral behavior of the emission cross section. All data are normalized.

This figure shows that the Brendel-Bormann model reproduces the spectral dependance and Stokes shift that was already observed experimentally by several groups [40,60]. It shows that the Lorentzian model cannot be used to compute the photoluminescent emission. We will show in this article the procedure to obtain the parameters of the Brendel-Bormann model in order to compute with precision the photoluminescent emission. We will also discuss why this model is well-suited for photoluminescence calculations.

2. Experimental measurements

The fluorophore considered in this article is a J-aggregated dye (TDBC) deposited on a thin (50 nm) continuous silver film thermally evaporated on a glass substrate. A highly concentrated ($8.75\ 10^{-3}$ mol.L^{-1}) aqueous solution of TDBC is spin coated on a silver film to form a 17 nm-thick continuous layer. The sample is investigated through photoluminescence and reflectometry measurements from the glass side as shown in Fig. 3(a). For this purpose, the sample sits on an inverted microscope. The objective's back-focal plane is imaged onto the slit of a spectrometer coupled to an EMCCD camera. The resulting images are resolved both in energy and in-plane wavevector [61]. For reflectometry measurements, white thermal light is focused on the sample through the objective. For photoluminescence measurements, a 445 nm laser is used. A polarizer is inserted on the detection path to select the Transverse Magnetic (TM) polarization of the signal.

An example of reflectivity map is given in Fig. 3(b). It is seen that there is a dip due to the resonant excitation of a surface plasmon at the interface metal/TDBC. The presence of a gap is the signature of strong coupling between the surface plasmon and the TDBC so that polaritons are formed. An example of photoluminescence map is given in Fig. 1(a) where the map displays emission peaks at the same frequency and angular dependence than the reflectivity dip. This points to a mechanism of emission assisted by the polaritons. First, TDBC molecules relax by emitting a polariton. The leakage of the polariton into glass generates the observed photoluminescence. We note that the upper polariton is clearly seen in reflection but hardly seen in photoluminescence. We will explain this feature in the next section.

Optical Materials EXPRESS

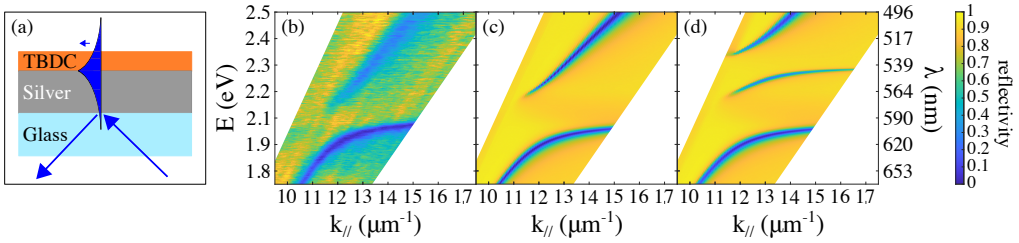

Fig. 3. Reflectivity maps of a 17-nm-thick layer of TDBC on a 50-nm-thick layer of silver: (a) Structure of the sample illuminated from glass in Kretschmann geometry, leading to a surface plasmon excitation (b) Experimental data, (c) Simulated reflectivity map for an anisotropic model of TDBC permittivity and (d) Simulated reflectivity map for an isotropic model of TDBC permittivity. Simulation realized with a Brendel-Bormann model, after optimization on photoluminescence. All data gathered in Table 1.

3. Data analysis

3.1. Methods

3.1.1. Cost function

The purpose of the paper is to obtain an accurate model of the permittivity $\epsilon_{\text{model}}(p_1, p_2, \ldots)$ of TDBC by fitting its parameters $p_1, p_2, \ldots$ of the permittivity model. We aim at fitting theoretically the experimental emitted power $P_{\text{em}}^{\text{exp}}(\theta, \lambda)$ such that:

$$P_{\text{em}}^{\text{exp}}(\theta, \lambda) = P_{\text{em}}^{\text{th}}(\theta, \lambda, \epsilon_{\text{model}}(p_1, p_2, \ldots)), \tag{1}$$

where $P_{\text{em}}^{\text{th}}$ is the theoretical emitted power, which depends on the dielectric permittivity model $\epsilon_{\text{model}}(p_1, p_2, ..)$. We identify the parameters with an optimization procedure based on the cost function $f_{\text{cost}}(\epsilon)$:

$$\text{f}_{\text{cost}}(\epsilon_{\text{model}}) = \sum_{\theta_i=1}^{N} \sum_{\lambda_j=1} [P_{\text{em}}^{\text{exp}}(\theta_i, \lambda_j) - P_{\text{em}}^{\text{th}}(\theta_i, \lambda_i, \epsilon_{\text{model}}(\lambda_j, p_1, p_2, \ldots))]^2. \tag{2}$$

3.1.2. Kirchhoff law

The theoretical emitted power $P_{\text{em}}^{\text{th}}$ is computed using the local Kirchhoff law [62]. It states that the emitted power dP_e at a wavelength λ, emitted by a layer of thermalized emitters in the direction $\mathbf{u}$ (i.e. for a given angle θ) and a given polarization state l can be cast in the form:

$$dP_e^{(l)}(\mathbf{u}, \lambda) = d\lambda d\Omega \int_V d^3\mathbf{r}' \alpha^{(l)}(-\mathbf{u}, \mathbf{r}', \lambda) \frac{hc^2}{\lambda^5} \frac{1}{\exp(\frac{hc}{\lambda k_B T} - \frac{\mu}{k_B T}) - 1}, \tag{3}$$

where $\alpha^{(l)}(-\mathbf{u}, \mathbf{r}', \lambda)\, \varphi_{\text{inc}}\, d^3\mathbf{r}'$ is the absorption in a volume element $d^3\mathbf{r}'$ of the emitting layer illuminated by an incident plane wave in the $-\mathbf{u}$ direction with a given polarization l and a power flux per unit area φ_{inc}. T is the temperature and μ is the photon chemical potential which depends on the pumping of TDBC.

The model accounts for the observed correlation between the minimum of the reflectivity and the maximum of emission. Indeed, for an opaque body, an increased absorptivity due to surface waves excitation leads to a reduced reflectivity. Hence, the model accounts for enhanced emission due to the excitation of surface plasmons through the absorptivity term. The model also explains why the upper polariton is observed in reflectivity but hardly seen in photoluminescence. The key difference between both polaritons in emission is due to the Wien term $\exp(-\hbar\omega/k_B T)$ so that

Optical Materials EXPRESS

emission at high frequencies is reduced. Just like the Stokes shift, this difference can be seen as a consequence of the exponentially decaying occupation of excited states for a thermalized system.

3.1.3. Brendel-Bormann model: a suitable model to account for the photoluminescence

It is necessary to be able to compute the absorption in the emitting layer in order to obtain the emitted power, and consequently to have an appropriate dielectric permittivity model. As shown in Fig. 1 or in Fig. 2(b), a Lorentzian model, commonly used for dye molecules such as TDBC, is not able to reproduce the experimental photoemission. In particular, it is clearly seen in Fig. 2(b) that the imaginary part of the permittivity should decay much faster than for a Lorentzian at large wavelengths. In this article, we use the Brendel-Bormann model [54–56] for the dielectric permittivity:

$$\epsilon(\omega) = \epsilon_{\mathrm{bg}} + \sum_{k=1}^{m} X_{\mathrm{k}}(\omega), \tag{4}$$

with X_{k} an infinite sum of Lorentz oscillators whose amplitudes are given by a Gaussian function:

$$X_{\mathrm{k}}(\omega) = \frac{1}{\sqrt{2\pi}\sigma_{\mathrm{k}}} \int_{-\infty}^{+\infty} dx \exp\left(-\frac{(x-\nu_{0\mathrm{k}})^2}{2\sigma_{\mathrm{k}}^2}\right) \frac{\nu_{\mathrm{pk}}^2}{x^2 - \omega^2 - i\nu_{\tau\mathrm{k}}\omega}. \tag{5}$$

In order to compute it numerically, we use the formalism and the formula defined in [55].

This model provides a function of the complex variable ω which is analytical in a complex half-space so that it satisfies Kramers-Kronig relations by construction. The Gaussian distribution of oscillators with frequency x and width $\nu_{\tau k}$ is a model for the distribution of transitions between the rovibrational states of two electronic levels. As a consequence of the distribution of oscillators accounted by the Gaussian function, any incident frequency ω is resonant with only a small fraction $\nu_{\tau\, k}/\sigma_k$ of the transitions, so that the imaginary part can be drastically reduced as compared with a simple oscillator. In other words, a Lorentzian model accounts for the homogeneous broadening of a single transition between two states, whereas the Brendel-Bormann model accounts for the inhomogeneous broadening due to a large number of narrow transitions between two bands.

3.1.4. Data processing

Before performing the optimization procedure, we first filter some noise on the experimental photoluminescence map data. First of all, the signal of the emission map is convoluted with a 3-by-3 matrix of ones. Secondly, the background contribution is evaluated by averaging the value of the signal far from the emission area in a square between -30° and +30° and between 520 nm and 560 nm. This average value is then subtracted from the photoluminescence signal.

In the optimization procedure, the following assumptions are made. Firstly, the medium, the chemical potential μ and the temperature T are all considered to be homogeneous within the entire volume of the layer. Secondly, Wien's approximation is valid at 300K: $\exp(\frac{\hbar\omega-\mu}{k_B T})>>1$. With these assumptions, and after normalization by the maximum emitted power at λ_0, Eq. (3) can be simplified:

$$\frac{dP_e^{(l)}(\mathbf{u},\lambda)}{dP_e^{(l)}(\mathbf{u},\lambda_0)} = \frac{dP_{abs}(-\mathbf{u},\lambda)\mathrm{I_{BB}}(\lambda)}{dP_{abs}(-\mathbf{u},\lambda_0)\mathrm{I_{BB}}(\lambda_0)}, \tag{6}$$

with

$$\mathrm{I_{BB}}(\lambda) = \frac{1}{\lambda^5}\frac{1}{\exp(\frac{hc}{\lambda k_B T})}, \tag{7}$$

and

$$dP_{abs}(-\mathbf{u},\lambda) = \varphi_{\mathrm{inc}} \int_V d^3\mathbf{r}'\alpha^{(l)}(-\mathbf{u},\mathbf{r}',\lambda) \tag{8}$$

Optical Materials EXPRESS

To model our system, we can first choose the permittivity to be isotropic. The photoluminescence map therefore displays an additional mode in the gap [63] in contrast with the experimental data (Fig. 3(b,d)). However, the TDBC displays some anisotropy, due to the formation of oriented aggregates when packing TDBC molecules together. To account for the anisotropy, we introduce an additional term of ϵ in the perpendicular direction of the layer (denoted $\epsilon_\perp$) as an additional parameter of the cost function $f_{\text{cost}}(\epsilon)$. With this feature included in our model, we retrieve the two branches of the experimental data (Fig. 3(b,c)).

The silver layer is described by a Drude model:

$$\epsilon_{\text{Ag}}(\omega) = \epsilon_\infty - \frac{\Omega_{\text{p}}^2}{\omega^2 + i\omega\gamma}, \tag{9}$$

with the following values to account for the data $\epsilon_\infty = 5$, $\Omega_{\text{p}} = 8.89$ eV and $\gamma = 0.1$ eV.

4. Results

4.1. Comparison of experimental and theoretical photoluminescence map

The experimental emission was correctly reproduced by the simulation as can be seen in Fig. 4 using $m = 3$ (see Eq. (4)). Both the experimental data and the simulations are obtained in the TM configuration. Note that the upper polariton branch in the experimental photoluminescence map fades into the detector noise. As a consequence, the optimization procedure is not completely able to assess its quantitative contribution to the permittivity. This explains the slight discrepancies between experimental and simulated data regarding the upper polariton (Fig. 3(b,c)).

The parameters of the refractive index model are shown in Table 1 and the associated permittivity and refractive index are plotted as a function of λ in Fig. 5. The results reported in Table 1 show that Lorentzian lines of the Brendel-Bormann model are much narrower than Gaussian lines ($\nu_{\tau\text{k}} \ll \sigma_{\text{k}}$) as expected for inhomogeneous broadening due to a large number of narrow transitions between rovibrational levels.

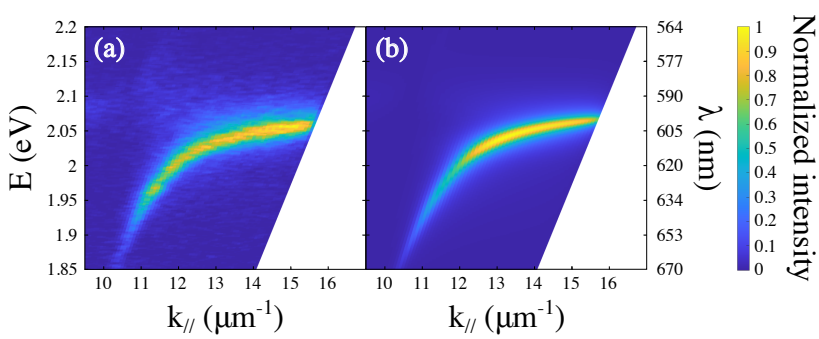

Fig. 4. Maps of photoluminescence as a function of the energy and the parallel wave-vector, normalized by their maximum values: (a) Experimental photoluminescent emission of TDBC and (b) simulated emission after optimization of the Brendel-Bormann model. All data are normalized by their maximum values.

When comparing with the literature on J-aggregated TDBC in solution [60,64], we observe a blue shift and a broadening of the emission and absorption spectra (Fig. 2(a)). As shown in [60], the monomer TDBC spectra are broader and strongly blue-shifted. An intermediate situation, similar to our observation, arises when the J-aggregates interact with their environment [64].

Optical Materials EXPRESS

Table 1. Brendel-Bormann model parameter values

Parameters	k=1	k=2	k=3
ν_{0k} (eV)	2.07	2.14	2.17
$\nu_{\tau k}$ (eV)	1.14e-09	1.46e-13	2.10e-06
ν_{pk} (eV)	0.10	1.44	0.25
σ_k (eV)	0.025	0.025	0.070
ϵ_{bg}		2.83	
$\epsilon_{\perp}$		2.82	

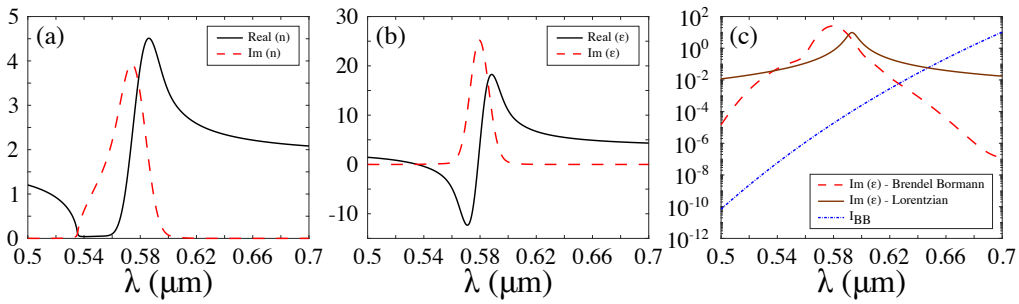

Fig. 5. (a) The complex refractive index n of TDBC obtained with a Brendel-Bormann model, (b) the complex dielectric permittivity ϵ of TDBC and (c) the imaginary part of the complex dielectric permittivity of TDBC obtained with a Brendel-Bormann model (red dashed line) or with a Lorentzian model (brown plain line) compared to the Planck function I_{BB} (blue dotted line).

4.2. Discussion

As said in the introduction, it is possible in principle to compute the emission cross section from the absorption cross section using $\sigma_{em}(\omega) = \sigma_{abs}(\omega)\exp[\hbar(\mu - \omega)/k_B T]$ and then retrieve the experimental Stokes shift. Yet, the model of permittivity has to be extremely accurate at the low energy tail of the absorption spectrum to capture correctly the decay of the absorption spectrum. While this tiny absorption does not affect reflectivity measurements, it becomes critical when computing photoluminescence as it is multiplied by an exponentially varying term $\exp(-\hbar\omega/k_B T)$. If we consider an emitting system at temperature 300 K (25 meV) with an emission region whose spectral width is on the order of 0.1 eV, the factor $\exp(-\hbar\omega/k_B T)$ varies from 1 to $e^4 \approx 55$ in this band. The Brendel-Bormann model precisely enables to account for a fast decay of the imaginary part of the permittivity at long wavelengths which can compensate the exponential increase of the Planck function. To illustrate quantitatively this behavior, we use a logarithmic scale to plot in Fig. 5(c) the imaginary part of the permittivity when using either the Lorentzian model or the Brendel-Bormann model. We also plot the Planck function. It is clearly seen that the slow decay of the Lorentzian model cannot compensate the increase of Planck function resulting in the unphysical divergence that is shown in Fig. 1 and Fig. 2.

5. Conclusion

We have shown that it is possible to model quantitatively the photoluminescence of TDBC mediated by surface plasmons. This is a very good example of light emission by an ensemble of emitters interacting with a resonant surface. The interplay between the two systems is accounted for by the local Kirchhoff law [62] which introduces the absorptivity in the TDBC layer. We have

Optical Materials EXPRESS

shown that simple permittivity models fail to enable the photoluminescence calculation using Kirchhoff. Using the Brendel-Bormann model, the parameters of the model were found by fitting the experimental emission. This model captures accurately the decay of the absorption spectrum at long wavelengths so that it can be used to compute light emission by fluorophores. These results pave the way to the design of complex metasurfaces to control light emission, creating novel light sources with new properties.

Funding. H2020 European Research Council (754387, Marie Sklodowska-Curie 754387); Agence Nationale de la Recherche (ANR-17-CE24-0046, ANR-18-CE30-0014); Labex (ANR-10-IDEX-0001-02 PSL*, ANR-10-LABX-24).

Disclosures. The authors declare no conflicts of interest.

Data availability. Data underlying the results presented in this paper are not publicly available at this time but may be obtained from the authors upon reasonable request.

References

1. H. Iwase, D. Englund, and J. Vučković, "Spontaneous emission control in high-extraction efficiency plasmonic crystals," Opt. Express **16**(1), 426–434 (2008).
2. S. Wedge, J. A. E. Wasey, W. L. Barnes, and I. Sage, "Coupled surface plasmon-polariton mediated photoluminescencefrom a top-emitting organic light-emitting structure," Appl. Phys. Lett. **85**(2), 182–184 (2004).
3. J. S. Biteen, D. Pacifici, N. S. Lewis, and H. A. Atwater, "Enhanced radiative emission rate and quantum efficiency in coupled silicon nanocrystal-nanostructured gold emitters," Nano Lett. **5**(9), 1768–1773 (2005).
4. C. Liu, V. Kamaev, and Z. V. Vardeny, "Efficiency enhancement of an organic light-emitting diode with a cathode forming two-dimensional periodic hole array," Appl. Phys. Lett. **86**(14), 143501 (2005).
5. E. Ozbay, "Plasmonics: Merging photonics and electronics at nanoscale dimensions," Science **311**(5758), 189–193 (2006).
6. W. L. Barnes, "Electromagnetic crystals for surface plasmon polaritons and the extraction of light from emissive devices," J. Lightwave Technol. **17**(11), 2170–2182 (1999).
7. S. Pillai, K. R. Catchpole, T. Trupke, G. Zhang, J. Zhao, and M. A. Green, "Enhanced emission from si-based light-emitting diodes using surface plasmons," Appl. Phys. Lett. **88**(16), 161102 (2006).
8. J. B. Khurgin, G. Sun, and R. A. Soref, "Enhancement of luminescence efficiency using surface plasmon polaritons: figures of merit," J. Opt. Soc. Am. B **24**(8), 1968–1980 (2007).
9. J. B. Khurgin, G. Sun, and R. A. Soref, "Electroluminescence efficiency enhancement using metal nanoparticles," Appl. Phys. Lett. **93**(2), 021120 (2008).
10. G. Sun, J. B. Khurgin, and R. A. Soref, "Plasmonic light-emission enhancement with isolated metal nanoparticles and their coupled arrays," J. Opt. Soc. Am. B **25**(10), 1748–1755 (2008).
11. K. Okamoto, I. Niki, A. Shvartser, Y. Narukawa, T. Mukai, and A. Scherer, "Surface-plasmon-enhanced light emitters based on ingan quantum wells," Nat. Mater. **3**(9), 601–605 (2004).
12. E. MS, M. K, Z. L, Y. E, and W. MC, *Proceedings of the National Academy of Sciences of the United States of America* 112, 1704–1709 (2014).
13. G. Lozano, S. R. Rodriguez, M. A. Verschuuren, and J. Gómez Rivas, "Metallic nanostructures for efficient led lighting," Light: Sci. Appl. **5**(6), e16080 (2016).
14. I. Gontijo, M. Boroditsky, E. Yablonovitch, S. Keller, U. K. Mishra, and S. P. DenBaars, "Coupling of ingan quantum-well photoluminescence to silver surface plasmons," Phys. Rev. B **60**(16), 11564–11567 (1999).
15. N. E. Hecker, R. A. Höpfel, and N. Sawaki, "Enhanced light emission from a single quantum well located near a metal coated surface," Physica E-low-dimensional Systems Nanostruct. **2**(1-4), 98–101 (1998).
16. J. Vuckovic, M. Loncar, and A. Scherer, "Surface plasmon enhanced light-emitting diode," IEEE J. Quantum Electron. **36**(10), 1131–1144 (2000).
17. A. Neogi, C.-W. Lee, H. O. Everitt, T. Kuroda, A. Tackeuchi, and E. Yablonovitch, "Enhancement of spontaneous recombination rate in a quantum well by resonant surface plasmon coupling," Phys. Rev. B **66**(15), 153305 (2002).
18. K. Guo, G. Lozano, M. A. Verschuuren, and J. Gómez Rivas, "Control of the external photoluminescent quantum yield of emitters coupled to nanoantenna phased arrays," J. Appl. Phys. **118**(7), 073103 (2015).
19. R. Paiella, "Tunable surface plasmons in coupled metallo-dielectric multiple layers for light-emission efficiency enhancement," Appl. Phys. Lett. **87**(11), 111104 (2005).
20. M. Decker, I. Staude, I. I. Shishkin, K. B. Samusev, P. Parkinson, V. K. A. Sreenivasan, A. Minovich, A. E. Miroshnichenko, A. Zvyagin, C. Jagadish, D. N. Neshev, and Y. S. Kivshar, "Dual-channel spontaneous emission of quantum dots in magnetic metamaterials," Nat. Commun. **4**(1), 2949 (2013).
21. H. Chen, J. Yang, E. Rusak, J. Straubel, R. Guo, Y. W. Myint, J. Pei, M. Decker, I. Staude, C. Rockstuhl, Y. Lu, Y. S. Kivshar, and D. Neshev, "Manipulation of photoluminescence of two-dimensional mose2 by gold nanoantennas," Sci. Rep. **6**(1), 22296 (2016).
22. A. Vaskin, J. Bohn, K. E. Chong, T. Bucher, M. Zilk, D.-Y. Choi, D. N. Neshev, Y. S. Kivshar, T. Pertsch, and I. Staude, "Directional and spectral shaping of light emission with mie-resonant silicon nanoantenna arrays," ACS Photonics **5**(4), 1359–1364 (2018).

Optical Materials EXPRESS

23. I. Staude, V. V. Khardikov, N. T. Fofang, S. Liu, M. Decker, D. N. Neshev, T. S. Luk, I. Brener, and Y. S. Kivshar, "Shaping photoluminescence spectra with magnetoelectric resonances in all-dielectric nanoparticles," ACS Photonics **2**(2), 172–177 (2015).
24. G. Vecchi, V. Giannini, and J. Gómez Rivas, "Shaping the fluorescent emission by lattice resonances in plasmonic crystals of nanoantennas," Phys. Rev. Lett. **102**(14), 146807 (2009).
25. J. Bohn, T. Bucher, K. E. Chong, A. Komar, D.-Y. Choi, D. N. Neshev, Y. S. Kivshar, T. Pertsch, and I. Staude, "Active tuning of spontaneous emission by mie-resonant dielectric metasurfaces," Nano Lett. **18**(6), 3461–3465 (2018).
26. S. Liu, A. Vaskin, S. Addamane, B. Leung, M.-C. Tsai, Y. Yang, P. P. Vabishchevich, G. A. Keeler, G. Wang, X. He, Y. Kim, N. F. Hartmann, H. Htoon, S. K. Doorn, M. Zilk, T. Pertsch, G. Balakrishnan, M. B. Sinclair, I. Staude, and I. Brener, "Light-emitting metasurfaces: Simultaneous control of spontaneous emission and far-field radiation," Nano Lett. **18**(11), 6906–6914 (2018).
27. T. Bucher, A. Vaskin, R. Mupparapu, F. J. F. Löchner, A. George, K. E. Chong, S. Fasold, C. Neumann, D.-Y. Choi, F. Eilenberger, F. Setzpfandt, Y. S. Kivshar, T. Pertsch, A. Turchanin, and I. Staude, "Tailoring photoluminescence from mos2 monolayers by mie-resonant metasurfaces," ACS Photonics **6**(4), 1002–1009 (2019).
28. A. F. Cihan, A. G. Curto, S. Raza, P. G. Kik, and M. L. Brongersma, "Silicon mie resonators for highly directional light emission from monolayer mos2," Nat. Photonics **12**(5), 284–290 (2018).
29. J. Liu, W. Wang, D. Wang, J. Hu, W. Ding, R. D. Schaller, G. C. Schatz, and T. W. Odom, "Spatially defined molecular emitters coupled to plasmonic nanoparticle arrays," Proc. Natl. Acad. Sci. **116**(13), 5925–5930 (2019).
30. H. Aouani, O. Mahboub, E. Devaux, H. Rigneault, T. W. Ebbesen, and J. Wenger, "Plasmonic antennas for directional sorting of fluorescence emission," Nano Lett. **11**(6), 2400–2406 (2011).
31. G. Lozano, D. J. Louwers, S. R. Rodríguez, S. Murai, O. T. Jansen, M. A. Verschuuren, and J. Gómez Rivas, "Plasmonics for solid-state lighting: enhanced excitation and directional emission of highly efficient light sources," Light: Sci. Appl. **2**(5), e66 (2013).
32. S. R. K. Rodriguez, G. Lozano, M. A. Verschuuren, R. Gomes, K. Lambert, B. De Geyter, A. Hassinen, D. Van Thourhout, Z. Hens, and J. Gómez Rivas, "Quantum rod emission coupled to plasmonic lattice resonances: A collective directional source of polarized light," Appl. Phys. Lett. **100**(11), 111103 (2012).
33. G. Lozano, G. Grzela, M. A. Verschuuren, M. Ramezani, and J. G. Rivas, "Tailor-made directional emission in nanoimprinted plasmonic-based light-emitting devices," Nanoscale **6**(15), 9223–9229 (2014).
34. L. Shi, X. Yuan, Y. Zhang, T. Hakala, S. Yin, D. Han, X. Zhu, B. Zhang, X. Liu, P. Törmä, W. Lu, and J. Zi, "Coherent fluorescence emission by using hybrid photonic–plasmonic crystals," Laser Photonics Rev. **8**(5), 717–725 (2014).
35. J. Bellessa, C. Bonnand, J. C. Plenet, and J. Mugnier, "Strong coupling between surface plasmons and excitons in an organic semiconductor," Phys. Rev. Lett. **93**(3), 036404 (2004).
36. J. Dintinger, S. Klein, F. Bustos, W. L. Barnes, and T. W. Ebbesen, "Strong coupling between surface plasmon-polaritons and organic molecules in subwavelength hole arrays," Phys. Rev. B **71**(3), 035424 (2005).
37. D. E. Gómez, K. C. Vernon, P. Mulvaney, and T. J. Davis, "Surface plasmon mediated strong exciton-photon coupling in semiconductor nanocrystals," Nano Lett. **10**(1), 274–278 (2010).
38. S. Aberra Guebrou, C. Symonds, E. Homeyer, J. C. Plenet, Y. N. Gartstein, V. M. Agranovich, and J. Bellessa, "Coherent emission from a disordered organic semiconductor induced by strong coupling with surface plasmons," Phys. Rev. Lett. **108**(6), 066401 (2012).
39. L. Shi, T. K. Hakala, H. T. Rekola, J.-P. Martikainen, R. J. Moerland, and P. Törmä, "Spatial coherence properties of organic molecules coupled to plasmonic surface lattice resonances in the weak and strong coupling regimes," Phys. Rev. Lett. **112**(15), 153002 (2014).
40. J. George, S. Wang, T. Chervy, A. Canaguier-Durand, G. Schaeffer, J.-M. Lehn, J. A. Hutchison, C. Genet, and T. W. Ebbesen, "Ultra-strong coupling of molecular materials: spectroscopy and dynamics," Faraday Discuss. **178**, 281–294 (2015).
41. P. Törmä and W. L. Barnes, "Strong coupling between surface plasmon polaritons and emitters: a review," Rep. Prog. Phys. **78**(1), 013901 (2015).
42. J. George, T. Chervy, A. Shalabney, E. Devaux, H. Hiura, C. Genet, and T. W. Ebbesen, "Multiple rabi splittings under ultrastrong vibrational coupling," Phys. Rev. Lett. **117**(15), 153601 (2016).
43. S. R. K. Rodriguez, J. Feist, M. A. Verschuuren, F. J. Garcia Vidal, and J. Gómez Rivas, "Thermalization and cooling of plasmon-exciton polaritons: Towards quantum condensation," Phys. Rev. Lett. **111**(16), 166802 (2013).
44. T. K. Hakala, A. J. Moilanen, A. I. Väkeväinen, R. Guo, J.-P. Martikainen, K. S. Daskalakis, H. T. Rekola, A. Julku, and P. Törmä, "Bose–einstein condensation in a plasmonic lattice," Nat. Phys. **14**(7), 739–744 (2018).
45. A. Vaskin, R. Kolkowski, A. F. Koenderink, and I. Staude, "Light-emitting metasurfaces," Nanophotonics **8**(7), 1151–1198 (2019).
46. L. Ferraioli, P. Maddalena, E. Massera, A. Parretta, M. A. Green, A. Wang, and J. Zhao, "Evidence for generalized kirchhoff's law from angle-resolved electroluminescence of high efficiency silicon solar cells," Appl. Phys. Lett. **85**(13), 2484–2486 (2004).
47. P. Würfel, "The chemical potential of radiation," J. Phys.C: Solid State Phys. **15**(18), 3967–3985 (1982).
48. M. A. Green, J. Zhao, and A. e. a. Wang, "Efficient silicon light-emitting diodes," Nature **412**(6849), 805–808 (2001).
49. I. Shlesinger, H. Monin, J. Moreau, J. Hugonin, M. Dufour, S. Ithurria, B. Vest, and J.-J. Greffet, "Strong coupling of nanoplatelets and surface plasmons on a gold surface," ACS Photonics **6**(11), 2643–2648 (2019).

Optical Materials EXPRESS

50. K. Takatori, T. Okamoto, K. Ishibashi, and R. Micheletto, "Surface exciton polaritons supported by a j-aggregate-dye/air interface at room temperature," Opt. Lett. **42**(19), 3876–3879 (2017).
51. M. Garcia-Vergara, G. Demésy, and F. Zolla, "Extracting an accurate model for permittivity from experimental data: hunting complex poles from the real line," Opt. Lett. **42**(6), 1145–1148 (2017).
52. Z.-Z. Gu, S. Hayami, Q.-B. Meng, T. Iyoda, A. Fujishima, and O. Sato, "Control of photonic band structure by molecular aggregates," J. Am. Chem. Soc. **122**(43), 10730–10731 (2000).
53. Y. U. Lee, E. Garoni, H. Kita, K. Kamada, B. H. Woo, Y. C. Jun, S. M. Chae, H. J. Kim, K. J. Lee, S. Yoon, E. Choi, F. Mathevet, I. Ozerov, J. C. Ribierre, J. W. Wu, and A. D'Aléo, "Strong nonlinear optical response in the visible spectral range with epsilon-near-zero organic thin films," Adv. Opt. Mater. **6**(14), 1701400 (2018).
54. R. Brendel and D. Bormann, "An infrared dielectric function model for amorphous solids," J. Appl. Phys. **71**(1), 1–6 (1992).
55. A. D. Rakić, A. B. Djurišić, J. M. Elazar, and M. L. Majewski, "Optical properties of metallic films for vertical-cavity optoelectronic devices," Appl. Opt. **37**(22), 5271–5283 (1998).
56. A. Djorović, M. Meyer, B. L. Darby, and E. C. Le Ru, "Accurate modeling of the polarizability of dyes for electromagnetic calculations," ACS Omega **2**(5), 1804–1811 (2017).
57. Y. B. Band and D. F. Heller, "Relationships between the absorption and emission of light in multilevel systems," Phys. Rev. A **38**(4), 1885–1895 (1988).
58. D. Sawicki and R. Knox, "Universal relationship between optical emission and absorption of complex systems: An alternative approach," Phys.Rev.A **54**(6), 4837–4841 (1996).
59. C. Henry and F. Kazarinov, "Quantum noise in photonics," Rev. Mod. Phys. **68**(3), 801–853 (1996).
60. D. G. Lidzey and D. M. Coles, *Strong Coupling in Organic and Hybrid-Semiconductor Microcavity Structures* (Springer International Publishing, Cham, 2015), pp. 243–273.
61. K. Chevrier, J. M. Benoit, C. Symonds, S. K. Saikin, J. Yuen-Zhou, and J. Bellessa, "Anisotropy and controllable band structure in suprawavelength polaritonic metasurfaces," Phys. Rev. Lett. **122**(17), 173902 (2019).
62. J.-J. Greffet, P. Bouchon, G. Brucoli, and F. m. c. Marquier, "Light emission by nonequilibrium bodies: Local kirchhoff law," Phys. Rev. X **8**, 021008 (2018).
63. E. Bailly, J.-P. Hugonin, B. Vest, and J.-J. Greffet, "Spatial coherence of light emitted by thermalized ensembles of emitters coupled to surface waves," Phys. Rev. Research **3**(3), L032040 (2021).
64. D. L. Akins, "Enhanced raman scattering by molecular nanoaggregates," Nanomaterials and Nanotechnology **4**, 4 (2014).